LA-UR-98-306

HANDBOOK OF SCIENCE ALGORITHMS FOR THE MULTISPECTRAL THERMAL IMAGER

Barham W. Smith, Editor

Christoph C. Borel, William B. Clodius, Anthony B. Davis, Pawel Smolarkiewicz, John J. Szymanski, James Theiler, and Pierre V. Villeneuve

Nonproliferation and International Security Division
Los Alamos National Laboratory

Alfred Garrett and Lance O'Steen

Savannah River Technical Center

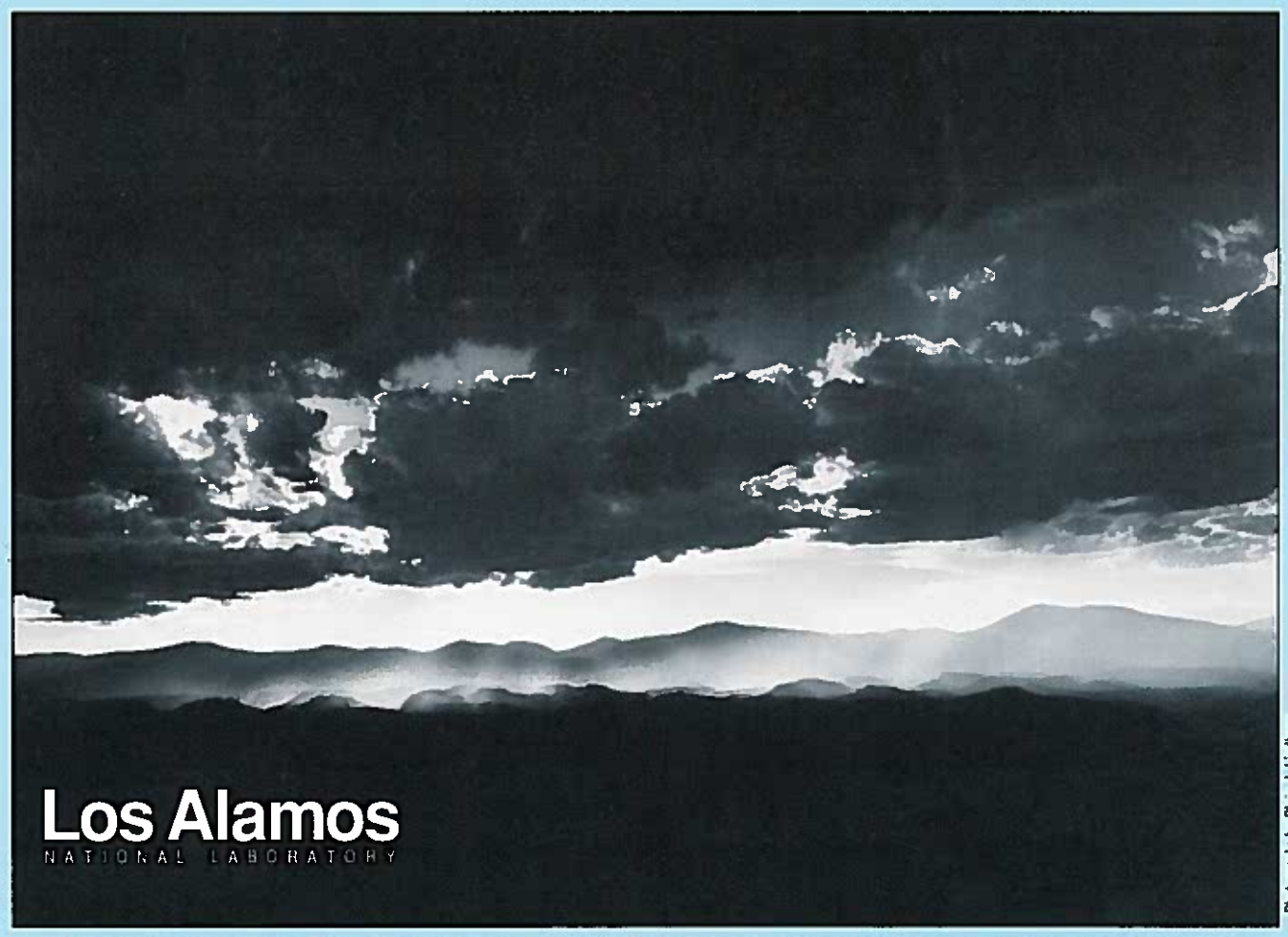

Photograph: by Chris J. Lindberg

M T I

Handbook of Science Algorithms

for the Multispectral Thermal Imager

Version 2, May 20, 1998

Prepared by the MTI Modeling and Science Team

Los Alamos National Laboratory
and Savannah River Technology Center

Barham W. Smith, Editor

Contributors to the Document

CHRISTOPH C. BOREL
Los Alamos National Laboratory
Mail Stop C-323
Los Alamos, NM 87545
Phone: 505-667-8972
Email: cborel@lanl.gov
Fax: 505-667-3815

WILLIAM B. CLODIUS
Los Alamos National Laboratory
Mail Stop C-323
Los Alamos, NM 87545
Phone: 505-665-9370
Email: wclodius@lanl.gov
Fax: 505-667-3815

ANTHONY B. DAVIS
Los Alamos National Laboratory
Mail Stop C-323
Los Alamos, NM 87545
Phone: 505-665-6577
Email: adavis@lanl.gov
Fax: 505-667-3815

ALFRED GARRETT
Savannah River Technical Center
Aiken, SC
Phone: 803-725-4870
Email: alfred.garrett@srs.gov
Fax: 803-725-4704

LANCE O'STEEN
Savannah River Technical Center
Aiken, SC
Phone: 803-725-2449
Email: alfred.garrett@srs.gov
Fax: 803-725-3272

BARHAM W. SMITH, Team Leader
Los Alamos National Laboratory
Mail Stop C-323
Los Alamos, NM 87545
Phone: 505-667-1585
Email: bwsmith@lanl.gov
Fax: 505-667-3815

PAWEL SMOLARKIEWICZ
Los Alamos National Laboratory
Mail Stop C-323
Los Alamos, NM 87545
Phone: 505-667-1585
Email: pawel@lanl.gov
Fax: 505-667-3815

JOHN J. SZYMANSKI
Los Alamos National Laboratory
Mail Stop C-323
Los Alamos, NM 87545
Phone: 505-665-9371
Email: szymanski@lanl.gov
Fax: 505-667-3815

JAMES THEILER
Los Alamos National Laboratory
Mail Stop D-436
Los Alamos, NM 87545
Phone: 505-665-5682
Email: jt@lanl.gov
Fax: 505-665-4414

PIERRE V. VILLENEUVE
Los Alamos National Laboratory
Mail Stop C-323
Los Alamos, NM 87545
Phone: 505-667-7739
Email: pierre@nis.lanl.gov
Fax: 505-667-3815

Acknowledgements

Many people have contributed over the years to the development of science algorithms for MTI. The team would like to thank: the Project Scientist, Paul Weber; the calibration team leader, Steve Bender; past postdoctoral associates Carmen Tornow and Bradley G. Henderson; past modeling and analysis team members, including Brad Cooke, Bill Powers, Jack Hills, Andrew Zardecki, George Auchampaugh, Bryan Laubscher, and Paul Pope; visiting scientist Veronique Carrére; colleagues from our partner DOE Laboratories, including Mal Pendergast and Phil Thacher; and past students, including Tony Crider, Jennifer Johnson, and Daniel Schläpfer.

The Multispectral Thermal Imager project is a joint effort of Sandia National Laboratory, Los Alamos National Laboratory, and Savannah River Technical Center, and is funded by the U. S. Department of Energy's Office of Research and Development.

TABLE OF CONTENTS

TABLE OF CONTENTS

TABLE OF CONTENTS

TABLE OF CONTENTS

TABLE OF ACRONYMS

The acronyms used in this report are defined in the following table.

TABLE A. List of Acronyms

Acronym	Name	Meaning
ADA	Aperture Door Assembly	The high emissivity door at the external aperture of the MTI optical assembly that serves as a thermal infrared calibration source.
APDA	Atmospheric Pre-corrected Differential Absorption	A columnar water vapor retrieval method.
ARM	Atmospheric Radiation Measurement Program.	A DOE program intended to improve the parameterization used in cloud and climate models.
AVIRIS	Airborne Visible Infrared Imaging Spectrometer	A NASA airborne hyperspectral instrument.
BRDF	Bi-directional Reflectance Distribution Function	The dependence of reflectance on the source and detector locations.
CART	Cloud and Radiation Testbed	A collection of sites that serve as the primary focus of the DOE AM measurement program.
CIBR	Continuum Interpolated Band Ratio	A columnar water vapor retrieval method.
CPU	Central Processing Unit	The main processor in an electronic computing system.
CW	Columnar Water Vapor	The integrated water vapor content of the atmosphere in a vertical column.
DEM	Digital Elevation Model	A representation of the topography of a surface.
DLG	Digital Line Graph	A representation of the topography of a surface.
DN	Digital Number	Quantified instrument response.
DoD	Department of Defense	A cabinet level department within the US government.
DOE	Department of Energy	A cabinet level department within the US government.
ENVI	Environment for the Visualization of Images	An IDL based image data analysis environment.
EOS	Earth Observing System	The Earth orbiting satellite component of MTPE.
FOV	Field of View	The solid angle subtended by a pixel, or array of pixels, using geometrical optics.
FPA	Focal Plane Array	Photodetector arrays used in imaging systems.
GCM	Global Circulation Models	Computer models that serve as the basis of climate models.
GPS	Global Positioning System	A DoD satellite system that provides radio beacons that can be used to accurately determine the location of a receiver.
GSD	Ground Sampling Distance	The distance between pixel positions when mapped to the ground surface at nadir.
IDL	Interactive Data Language	The programming language used to implement most of the MTI algorithm's.

TABLE OF ACRONYMS

LANL	Los Alamos National Laboratory	A DOE laboratory.
LIDAR	Light Detection and Ranging	A remote sensing technique relying on the detection of backscattered laser light.
LIS	Logical Image Structure	A set of three two dimensional arrays, representing the image data associated with a given band and image acquisition.
LST	Land Surface Temperature	An estimate of the temperature of a segment of a land surface.
LWIR	Long Wave Infrared	The spectral range that includes the atmospheric window from 8 to 13.5 μm.
MAS	MODIS Airborne Simulator	A NASA airborne hyperspectral instrument.
M/EDPH	MTPE/EOS Data Products Handbook	NASA's documents describing the MTPE and EOS data products.
MEM	Maximum Entropy Method	An algorithm use to improve the spatial resolution of images.
MODIS	Moderate Resolution Imaging Spectrometer	A planned NASA satellite based multispectral imaging system.
MTF	Modulation Transfer Function	A measure of the resolution performance of an imaging system.
MTI	Multispectral Thermal Imager	A DOE satellite based multispectral imaging system.
MTIDB	MTI Data Base	The database maintained at MTI-DPAC.
MTI-DPAC	MTI Data Processing and Analysis Center	The facility where MTI data will undergo analysis before distribution.
MTISOC	MTI Satellite Operations Center	The MTI facility which performs traditional flight operations, mission support, and downlink capabilities.
MTPE	Mission to Planet Earth	A NASA remote sensing program emphasizing the collection of environmental data.
MWIR	Mid–Wave Infrared	The spectral range that includes the atmospheric window from 3.4 to 5.5 μm.
NASA	National Aeronautics and Space Administration	A department level branch of the U. S. government
NDVI	The normalized digital vegetation index	A measure of vegetation health based on data in the VNIR bands.
NIR	Near Infrared	The spectral range from about 0.7 μm to about 1.5 μm.
OBCS	On Board Calibration System	The internal calibration system component of the MTI payload.
PC	Principal Components	A transformation an image to a system where the covariance about the mean is diagonal.
PSF	Point Spread Function	A measure of the resolution performance of an imaging system.

TABLE OF ACRONYMS

PW	Precipitable Water	The integrated water vapor content of the atmosphere in a vertical column, in units of cm of surface water if precipitated out of the atmosphere.
RMS	Root Mean Square	A measure of the magnitude of a quantity.
RMSE	Root Mean Square Error	A measure of the magnitude of an error.
SCA	Sensor Chip Assembly	The grouping of MTI detector bands on the focal plane.
SNL	Sandia National Laboratory	A DOE research laboratory.
SNR	Signal to Noise Ratio	The ratio of signal to noise.
SRTC	Savannah River Technology Center	A DOE technical center.
SWIR	Short Wave Infrared	The spectral range from about 1.5 μm to about 3 μm.
TEE	Total Excess Energy	A measure of the additional energy in heated water.
TIMS	Thermal Infrared Multispectral Scanner	A NASA airborne multispectral instrument.
TIR	Thermal Infrared	Combined MWIR and LWIR spectral range.
TMS	Daedelus Thematic Mapper Simulator	An airborne hyperspectral instrument.
TOA	Top of Atmosphere	The effective top of atmosphere value of a quantity.
VIS	Visible	The spectral range from about 0.4 μm to about 0.7 μm.
USGS	United States Geological Survey	A bureau of the U. S. Department of the Interior.
VNIR	Visible to Near Infrared	The spectral range from about 0.4 μm to about 1.5 μm.
VRP	Visible Reflecting Panel	A panel that can be position at the external aperture of the MTI optical assembly with a uniform and robust high albedo surface to serve as a calibration source for the MTI solar reflecting bands.
WGS84	World Geodetic System 1984	A reference surface used in geo-registration.
WST	Water Surface Temperature	An estimate of the temperature of a water surface segment.

1. EXECUTIVE SUMMARY AND OVERVIEW OF DATA PRODUCTS

Barham W. Smith, William B. Clodius, and Christoph C. Borel

1.1 Overview

DOE's Multispectral Thermal Imager (MTI) program will demonstrate the performance of satellite-based multispectral imaging for proliferation detection. The MTI satellite is expected to be launched in late 1999 and begin operation after an initial checkout and degassing period. During its one year planned operational lifetime, it will obtain high quality data for a variety of sites of interest to the community. This document provides a summary of algorithms that will be used to process the MTI data. This section provides a summary of the MTI system and the notation used within this document, and an overview of the data products produced by the algorithms.

MTI is a multispectral pushbroom sensor imaging in fifteen bands from the visible into the long wave infrared. These bands are listed in Table1-1, along with a summary of satellite specifications for orbit, pointing, etc. Note that the MTI spacecraft is capable of taking a "look" at a target scene as it passes near the target zenith, then performing a pitch (and usually roll) maneuver to acquire a second look with the satellite at 50 to 60° from target zenith. Therefore a data collection during a single pass over a target will consist of one or two "looks", plus before- and after-look calibrations, plus ancillary data such as spacecraft position and orientation at the time of collection.

Image data in the fifteen bands, when combined with ancillary data from MTI and other sources, will be used to derive the Level 1 and Level 2 data products listed in Table 1-2. Level 4 data products, including some that are not produced at the MTI Data Processing and Analysis Center (MTI-DPAC) are listed in Table 1-3. Each data set is identified by its processing level followed by a short mnemonic. The processing levels are those from the EOS Reference Handbook [Barry and Varani 1995], except that Level 1B data is divided into two groups, Level 1B-U, for unregistered data, and Level 1B-R for coregistered data. The EOS Reference Handbook definition of these levels is given in Table 1-4. Products that rely on data in the solar-reflected bands are labeled "daytime". Products that are not expected to be available for each look with relevant data, because their derivation is expected to be analyst-intensive, are labeled "Non-standard". Some products that are easily derived from the data, e.g., effective reflectances, will be not be provided. The units to be used for the products are given in Table 1-5, while the notation to be used in the discussion of the algorithms is given in Table 1-6. Data flow diagrams are used in the discussions of data products. These diagrams use the conventions illustrated in Figure1-1.

Table 1-1. MTI Spectral Band Characteristics and Satellite Specifications

Band ID	Wavelength Range (μm)	Nominal Nadir GSD (m)	Detector Material	Description
A	0.45-0.52	5	Si-PIN	Blue "True Color"
B	0.52-0.60	5	Si-PIN	Green "True Color"
C	0.62-0.68	5	Si-PIN	Red "True Color"
D	0.76-0.86	5	Si-PIN	VNIR Vegetation
E	0.86-0.89	20	InSb	VNIR Water Vapor Reference
F	0.91-0.97	20	InSb	VNIR Water Vapor
G	0.99-1.04	20	InSb	VNIR Water Vapor Reference
H	1.36-1.39	40 (20)	InSb	VNIR Cirrus
I	1.54-1.75	20	InSb	SWIR Surface
J	3.49-4.10	20	InSb	MWIR Surface
K	4.85-5.05	20	InSb	MWIR Atmosphere
L	8.01-8.39	20	HgCdTe	LWIR Atmosphere
M	8.42-8.83	20	HgCdTe	LWIR Surface
N	10.15-10.7	20	HgCdTe	LWIR Surface
O	2.08-2.37	20	InSb	SWIR Surface

Operational Capabilities:		**System Parameters:**	
Orbit (at insertion)	545 ± 5 km	Registration:	
FOV (nadir)	12 x 12 km	within a scene	0.1 pixel
Cross-track pointing	± 20°	inter-band	0.5 smaller pixel
Along-track pointing	± 45°(±60° from target zenith)	Peak data rate	8 Mbit/sec
Site revisit time	avg. 1 week	Peak power	800 W
Local crossing times	1300 & 0100 hours ± 1 hour	Satellite mass	600 kg
Scan	Pushbroom	Aperture	36 cm
Mission lifetime	14 months with a goal of 3 years	Focal length	125.1 cm

On-board calibration system:		
Calibration wheel	Full-aperture calibrators	Vicarious calibrations
2 black bodies	High emissivity door	Deep space
Narcissus mirror	Sun-reflectance panel	Infrared stars
2 tungsten lamps		Ground truth sites

Focal plane array:			
Signal quantization	12 bits	FPA temperature	75 K

Table 1-2. List of MTI Level 1 and 2 Data Products

Product ID	Data Set Name	Notes
Level 0-Raw	Archival Data	
Level 0-DN	DN images in Logical Image Structure (LIS) format (all bands)	Subset of Level 0-Raw
Level 0-SOH	State of Health data	Subset of Level 0-Raw
Level 1A-Base	Annotated look data	Adds data for calibration and pointing corrections.
Level 1B-U	Unregistered Top of Atmosphere (TOA) radiances in LIS format (all bands)	Subset of Level 1A-Base
Level 1B-R-QL	Quick Look TOA data for browsing	Standard. Degraded resolution registered data.
Level 1B-R-Coreg	Co-registered TOA radiance cube at sensor	Standard; bands resampled to common grid.
Level 1B-R-Geo	Co-registered Geo-located TOA radiance cube	Standard; resampled and rubber sheeted.
Level 1B-R-Topo	Topographically co-registered and geo-located TOA radiance cube	Non-standard
Level 2-WM	Water Mask	Standard
Level 2-CirM	Cirrus Mask	Standard daytime
Level 2-CldM	Non-Cirrus Cloud Mask	Standard daytime
Level 2-Vap	Atmospheric Water Vapor Image	Standard daytime.
Level 2-WST-α	Water Surface Temperature	Standard. The optional "-α" suffix indicates the retrieval algorithm.[†]
Level 2-LST	Land Surface Temperature	Non-standard.
Level 2-Refl	Surface Reflectance cube corrected for atmosphere	Non-standard daytime.
Level 2-NDVI	The Normalized Difference Vegetation Index	Standard daytime
Level 2-Mat	Material Identification map	Non-standard daytime
Level 2-PC	Principal Components cube	Standard
Level 2-MNF	Minimum Noise Fraction cube	Standard
Level 2-IW	Iterative Wiener Filtered radiance cube	Non-standard
Level 2-MEM	Maximum Entropy Method filtered radiance cube.	Non-standard
Level 2-Pixon	Pixon based radiance cube	Non-standard

[†] α has the form M-L-T, with the allowed substitutions for M (method) being either R (robust) or P (physics), for L (looks) the numerals 1 or 2, and for T (time) either day or night.

Table 1-3. List of MTI Level 4 Data Products.

Product ID	Data Set Name	Notes
Level 4-ALGE	ALGE comparison data for water cooling systems	Non-standard
Level 4-RAMS	RAMS comparison data for cooling tower	Non-standard
Level 4-Subpix	Subpixel temperature analysis	Non-standard
Level 4-Veg	Vegetation Health Status map	Non-standard

Table 1-4. Data Set Processing Levels (from the *EOS Reference Handbook*)

Data Level	Description
Level 0	Reconstructed unprocessed instrument/payload data at full resolution: any and all communications artifacts (e.g., synchronization frames, communications headers) removed.
Level 1A	Reconstructed unprocessed instrument/payload data at full resolution, time referenced and annotated with ancillary information including geometric and radiometric calibration coefficients, and georeferencing parameters (i.e., satellite ephemeris, orientation, pixel positions) computed and appended, but not applied, to Level 0 data.
Level 1B	Level 1A data that has been processed to sensor units.
Level 2	Derived geophysical variables at the same resolution and location as the Level 1 source data.
Level 3	Variables mapped on uniform space-time grid scales.
Level 4	Model output or results from analyses of lower level data (i.e., variables described from multiple measurements).

Table 1-5. Units for product parameters

Parameter Name	Units	Comments
Brightness temperature	C	
Cirrus mask	—	
Clear sky mask	—	
Emissivity	—	Fractional
Geometric Parameters (WGS84 ellipsoid referenced)	Degree	Sun and view angles, Zenith angles, Azimuth angles (relative to local North)
Geographic latitude	Degree	Relative to WGS84 ellipsoid
Geographic longitude	Degree	Relative to WGS84 ellipsoid
Material Identifier	—	
Spectral Radiance	$W\ m^{-2}sr^{-1}\ \mu m^{-1}$	
Reflectance	—	Fractional
Scene elevation	M	Relative to WGS84 ellipsoid
Vegetation Health Status	—	Healthy, stressed, dead
Water mask	—	
Water surface temperature	C	
Water vapor	mm precipitable H_2O	

Table 1-6. Symbols, Nomenclature, and Units

Symbol	Description	Units
c	Speed of light in a vacuum	$m\ s^{-1}$
c_1	First radiation constant	$W\ cm^2$
c_2	Second radiation constant	cm K
DN	Digital number	—
h	Planck's constant	J s
I	Incidence [irradiance]	$W\ m^{-2}$
k	Boltzmann constant	$J\ K^{-1}$
k	Radian wavenumber	m^{-1}
L	Radiance, sterance	$W\ m^{-2}\ sr^{-1}$
M	Radiant exitance, emittance	$W\ m^{-2}$
O	Offset	—
P	Flux	$J\ s^{-1}$, W
R	Distance	m
R	Relative response	—
R	Radiance responsivity	$DN / (W\ m^{-2}\ sr^{-1})$
T	Temperature	K
U	Energy	J
u	Energy density	$J\ m^{-3}$
V	Voltage	V
α	Absorptance, absorptivity	—
$\alpha()$	Absorption coefficient	cm^{-1}
$\Delta\lambda$, $\Delta\nu$	Bandwidth	μm, cm^{-1}
ε	Emissivity	—
θ, ϕ	Polar, azimuthal angles	rad, deg
λ	wavelength	μm
ν	Wave number	cm^{-1}
ρ	Reflectance, reflectivity	—
τ	Transmissivity	—
τ_{OD}	Optical depth	—
Ω	Solid angle	sr
Superscripts:		
BB	Blackbody	
*	Effective	
Subscripts:		
B	Band	
D	Detector	
SL	Scene look	
V	Vicarious	
q	Photonic	
λ	wavelength	
ν	Wave number	

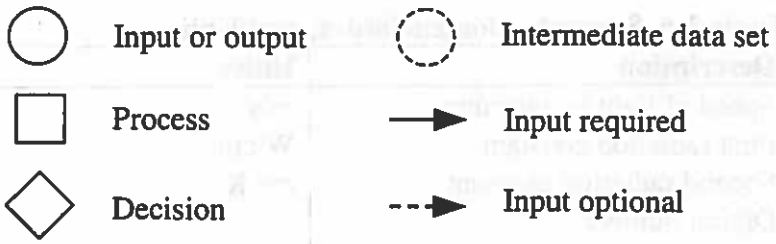

Figure 1-1. Data flow figure conventions

In the following sections we will give a short description of each of the major science algorithms that we intend to use to analyze and exploit MTI data. Before we begin that, we give an overview of the levels of data products and how they are defined.

The creation of MTI data products will be discussed in four parts:

- Archival storage ➜ Level 0-Raw
- Creation of a look base set ➜ Level 1A-Base
- Generation of co-registered band radiances ➜ Level 1B-R-β, where β stands for Coreg, Geo, or Top.
- Analysis ➜ Level 2-4

Products in each level depend on the output of the preceding level. There are additional interdependencies on products within the above levels.

1.2 Creation of Level 0 data

Raw MTI data, as it appears at the output channel of the ground station with all telemetry and encoding transformations removed, is a faithful copy of the contents of spacecraft memory. Because image records, calibration records, and state-of-health records are mixed in spacecraft memory, raw ground station data will immediately be reordered and stored in a more structured form, called Level 0. Because the next few processing steps, for example calibration correction, are highly dependent on the exact configuration and behavior of the MTI payload and spacecraft hardware, Level 0 by itself is unsuited for direct derivation of science products. Level 1A-Base will be much easier to use.

1. 2. 1 Level 0-DN: Digital number images in all bands

In order to discuss the archived image data it is necessary to summarize some of the characteristics of the MTI imaging system. The light-sensitive arrays are distributed over three identical Sensor Chip Assemblies (SCAs). Each SCA contains all fifteen bands laid out as linear pixel arrays across the SCA (see Figure 1-2) and acquires a pushbroom image covering about a third of the width of the MTI field of view (see Figure 1-3). The design results in great flexibility and robustness at the cost of a more complex registration problem.

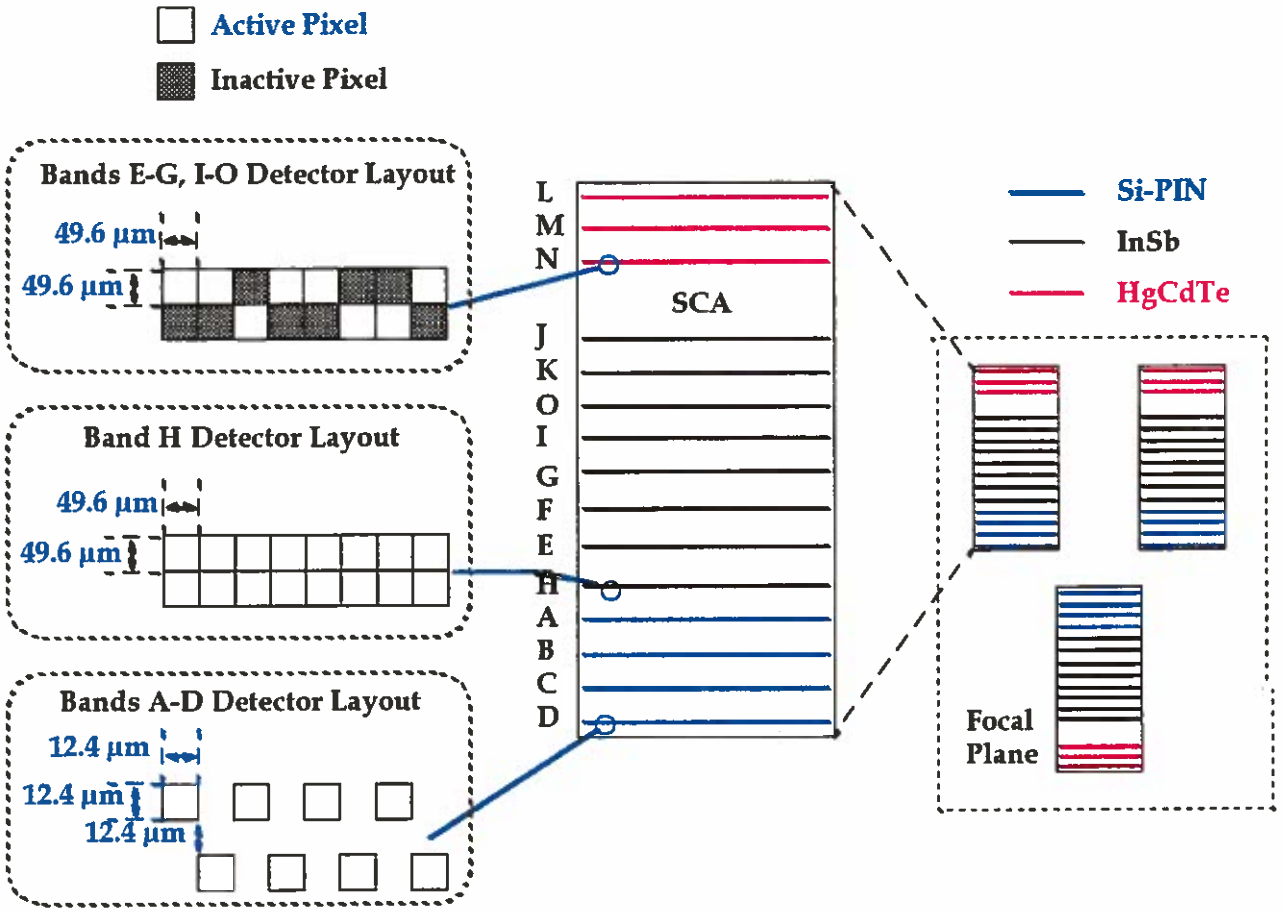

Figure 1-2. Layout of the MTI focal plane. Each of the sensor chip assemblies, or SCAs, has one linear array for each spectral band, fifteen in all. Near the center of the field of view, where the optical quality is highest, are the VNIR bands, whose arrays are silicon PIN diodes. The SWIR bands are next out, with indium antimonide photodiode arrays, and the TIR bands (HgCdTe semiconductor arrays) are farthest from the center, because the telescope is still nearly diffraction-limited at the edge of the field for those long wavelengths. The silicon semiconductor bands (A through D) have a staggered pixel layout as shown in the inset. The other bands have two pixels per location, only one of which can be selected, except for band H. Band H uses both rows of pixels to improve the signal-to-noise ratio. Thus for each band EFGIJKLMNO for each SCA, there is a binary map that tells which pixels were turned on for a given imaging sequence. This staggered pixel structure must be rectified to straight rows in processing.

The primary image data will be stored in a structure, termed Logical Image Structure (LIS), that reflects the layout of the imaging system. The LIS is a sequentially ordered "stack" of the readouts from one linear array. There will be one LIS for each band for each look. Each LIS will consist of three parts, one for each SCA. The layout of a typical LIS, and the associated band position on the SCA, is illustrated by Figure 1-3. As delivered to the user this data product will have an accompanying ENVI header for immediate display of the data.

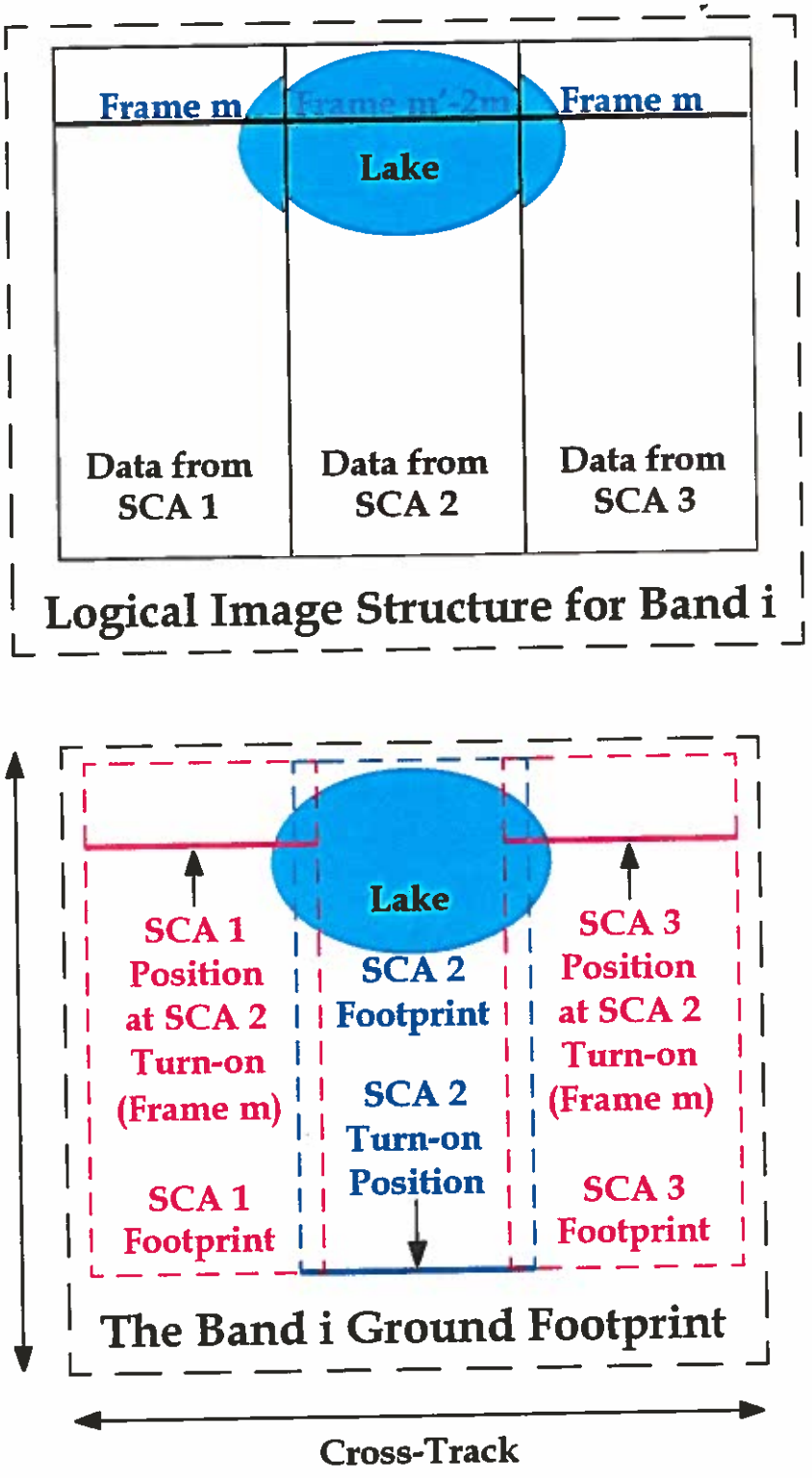

Figure 1-2. Diagram showing how the Logical Image Structure (LIS) for a single band corresponds to the ground footprint of the three-SCA focal plane array.

Level 0-DN is thus a compilation of the LISs for all bands, all three SCAs, for both looks and for both on-board calibrations. Light measurement or integration for each band of each SCA can be independently started and stopped. Typically an imaginary line will be drawn across the sub-satellite track, and integration in each band will be started when it crosses that line, and stopped when it crosses a second line beyond the target.

1. 2. 2 Level 0-SOH: State of Health Data

This data will be stored as sets of vector pairs, with one pair for each state of health parameter. Each pair consists of the parameter value with its associated time stamp. An IDL program will be provided to access and display this data.

1.3 Level 1A-Base: Annotated Look Data

The Level 1A-Base data set consists of ordered digital number data, Level 0-DN, to which has been appended such ancillary data as is necessary for the next steps in processing. The ancillary data has been appended but not been applied to the Level 0-DN set. In addition to look image data, Level 1A-Base includes the satellite ephemeris and orientation at the time of the look, time stamps, solar angles, the most pertinent calibration data, and state of health data during the calibrations and look. Level 1A-Base will also include our best calibration coefficients, derived from all information at our disposal, including historical ground calibration data, plus our estimates of the effects of component aging, the latest relative solar calibration, and the latest vicarious calibrations and deep space looks. This will allow interested users to compare their own calibration analysis to that of the project team.

Level 1A-Base is a data set designed for the "do-it-yourself" investigator.

1.4 Level 1B-U: Calibrated but Unregistered Band Radiances

Digital numbers generated by digital-to-analog conversion of the sensor element outputs are processed into scientific or physical units by application of the calibration coefficients. The result is Level 1B-U. See Section 2 for details. For now it is sufficient to show in Figure 1-4 how the next level of data is derived. Given Level 1A-Base data as in the left box, we apply a linear model for the response of each pixel to derive measured radiance units that are the basis for Level 1B-U, which, because it remains unregistered, retains the Logical Image Structure or LIS.

1. 5 Level 1B-R-β: Co-Registered Band Radiances

The generation of interpreted science products relies on the availability of co-registered and georegistered data. These data products are the foundation of the Level 2 data products described in this document, and can potentially be used by others to derive similar data products, or understand artifacts in their Level-2 data products. Because of its wide usage in the remote sensing community, geolocation will be given in terms of the U. S. Department of Defense World Geodetic System 1984 (WGS84) geocentric reference system, [Leick, 1990]. Geo-registration at the MTI-DPAC will be performed to a site-defined grid that is also defined in terms of WGS84.

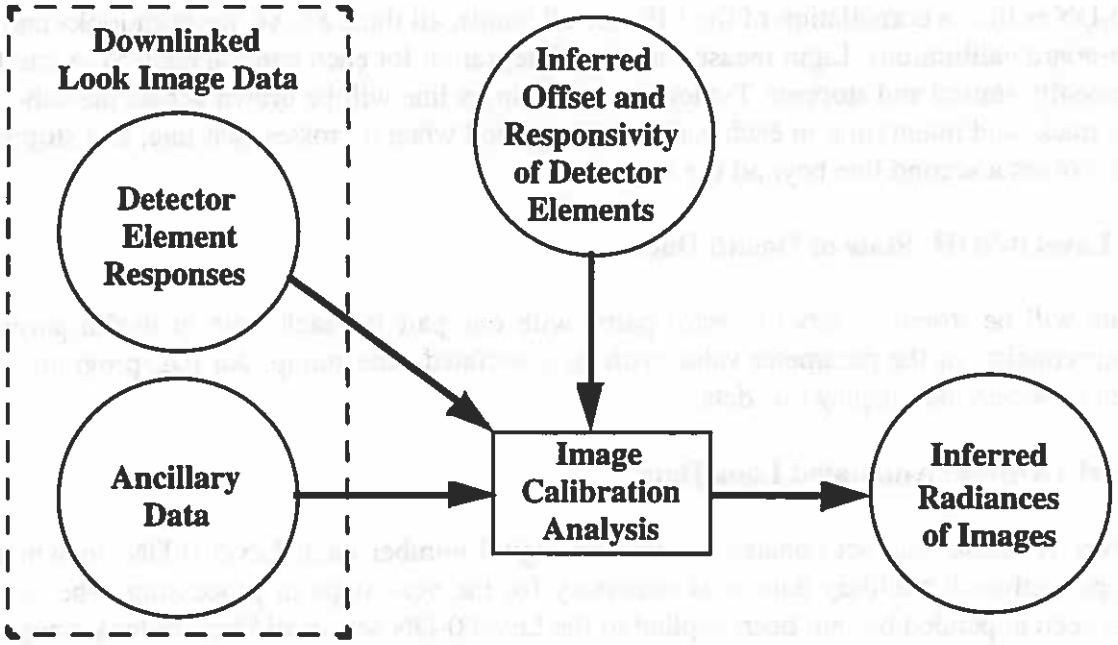

Figure 1-4. Generation of calibrated images. In the box at left, the look image data is of Level 1A-Base. Associated calibration data allows one to infer the calibration coefficients, which are applied to derive radiances, Level 1B-U.

Because it is not described elsewhere in this report, we will first summarize the general registration algorithm and then the products themselves.

1. 5. 1 Level 1B-R-β Algorithms

In order to move beyond the LIS data, it is necessary to reconstruct the movement of the instrument footprint across the ground. There are several steps to this procedure, each involving the determination of geometric factors and relationships between bands, SCAs and looks. While each step defines a transformation function, the transformation need not directly result in a resampling, and resampling at intermediate stages will be avoided to preserve spatial resolution.

Pointing knowledge will not be sufficiently tight to directly perform registration. The MTI bus will be capable of controlling pointing to ±0.19° in pitch and roll, ±0.15° in yaw. At an altitude of 550 km, this corresponds to ±1.8 km in pitch and roll at nadir. Absolute pointing knowledge will be ±1.7 km in both cross-track and along-track axes. For the second look at 55° pitch relative to the first look (about 60° from zenith at the target) pointing knowledge will be 2.8 km cross-track and 6.8 km along-track. All these performance numbers are 98% confidence. Uncorrected, this coarse pointing knowledge could lead to errors of hundreds of pixels, therefore in-scene methods of registration of look data are required.

The first step corrects for distortion of the FPA footprint by the optical assembly ("smile"). The second step co-registers a look's LIS data from different bands, making use of the fact that the FPA is a rigid body. This is described in Section 3 of this document. The result of this step is a

jitter function in the form of histories of along-track and cross-track motion as well as any rotation about the look vector. The jitter function allows resampling of all spectral bands onto a common grid. The third step geolocates the near-nadir look by selecting at least three control points in the image data that can be unambiguously associated with known locations on a map grid. The oblique look is co-registered to the near-nadir look by matching control points and then tweaking the resulting transformed image by cross-correlating it with the near-nadir look. If the topography is uneven at the target site, co-registration of the second look will be more difficult, and registration of the oblique look must take into account the three dimensional nature of the scene.

When all steps have been computed, the step-by-step mapping transformations will be convolved to produce a net transformation for each look that is used as the basis for a single resampling of the data using an optimum parametric interpolation.

1. 5. 2 Level 1B-R-β Products

Current plans are to provide the capability of performing several forms of registration based on the jitter analysis:

- Relative registration from the point of view of the MTI system;
- "Absolute" registration to a site defined height above WGS84, typically the mean height of a specific feature of interest in the scene;
- User-defined "absolute" registration to an arbitrary user defined height above WGS84;
- User-specified topographic geo-registration,

The definition of these surfaces is illustrated by Figure1-5. "Absolute" registration to a height above WGS84 has a potential inaccuracy of about one pixel due to errors in the inferred pointing, and tens of pixels in some parts of the scene due to a lack of detailed topographic information in the geo-registration process.

Relative registration from the point of view of the MTI system is implicitly provided by the jitter analysis. The Level 1B-R-Coreg data set is provided to the user community primarily because of its ease of generation/interpretation. It may be useful in understanding the source of problems in geolocated data. Because the look-angle distortions implicit in this data set complicate coregistration with images from other looks at a site, it is expected that the Level 1B-R-Coreg data set will rarely if ever serve as the basis of Level 2 products. However, Level 1B-R-QL, a degraded version of Level 1B-R-Coreg with only a subset of the spectral bands, will be available so that users can evaluate the potential of a given look without the financial or storage costs of obtaining a full image set.

Registration to a specified height above WGS84, Level 1B-R-Geo, provides a computationally straightforward first order correction to look-angle distortions. Co-registered radiances generated using this method are expected to allow quick comparisons of different looks and passes, and

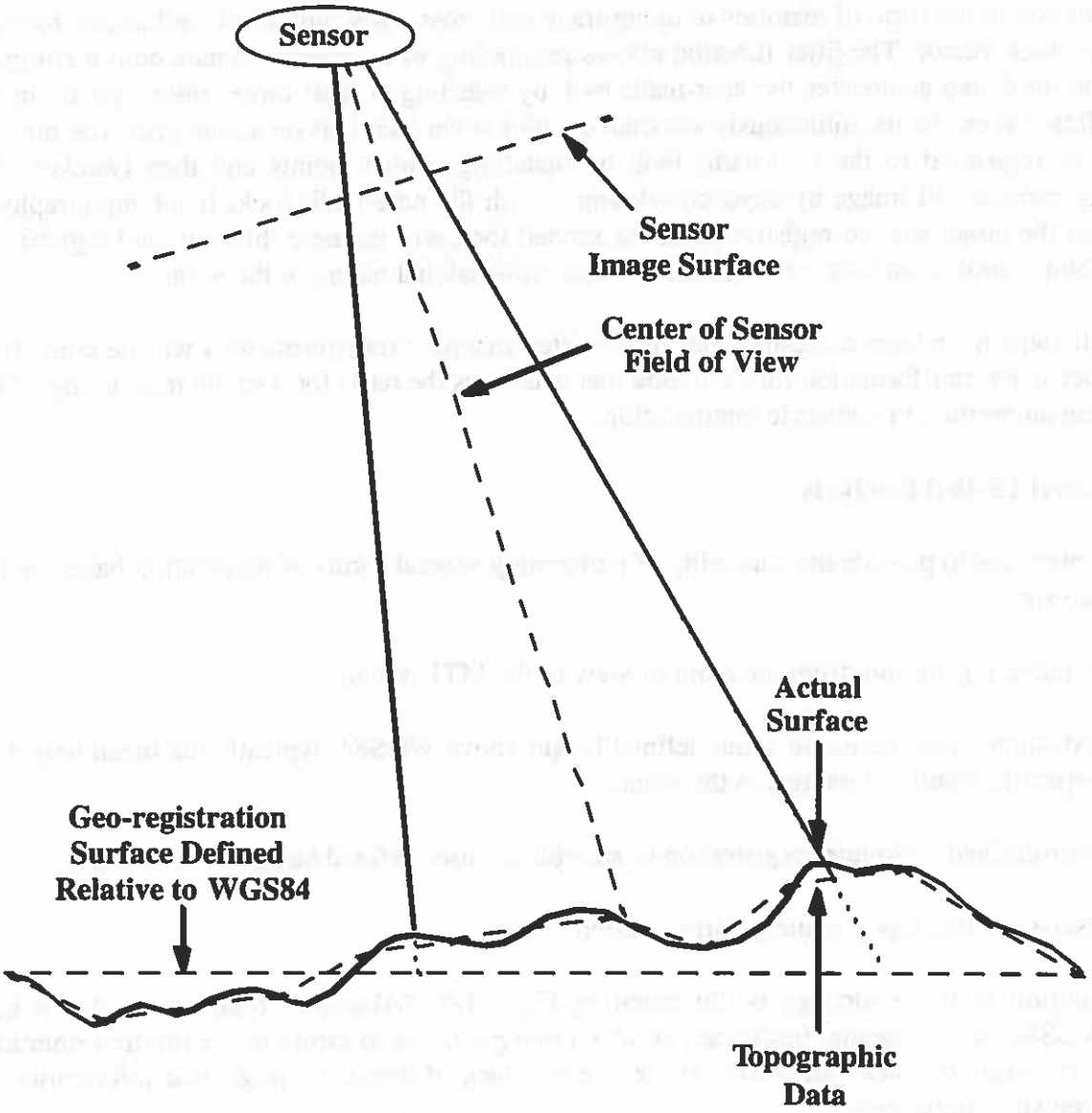

Figure 1-5. Illustration of the different possible image registration surfaces.

directly useful for near nadir looks, for very flat scenes, or horizontal components of scenes, e.g., still water bodies. It is expected that images generated using this method will serve as the basis of the majority of Level 2 products.

Registration to detailed topographic information, Level 1B-R-Topo, provides the ideal means of interpreting images. Unfortunately, topographic data at the sampling (five meters) and accuracy necessary to properly interpret MTI image data will not be available in most cases. Further, this mapping will require sub-pixel analyses for pixels that image surfaces, and detailed analyst intervention.

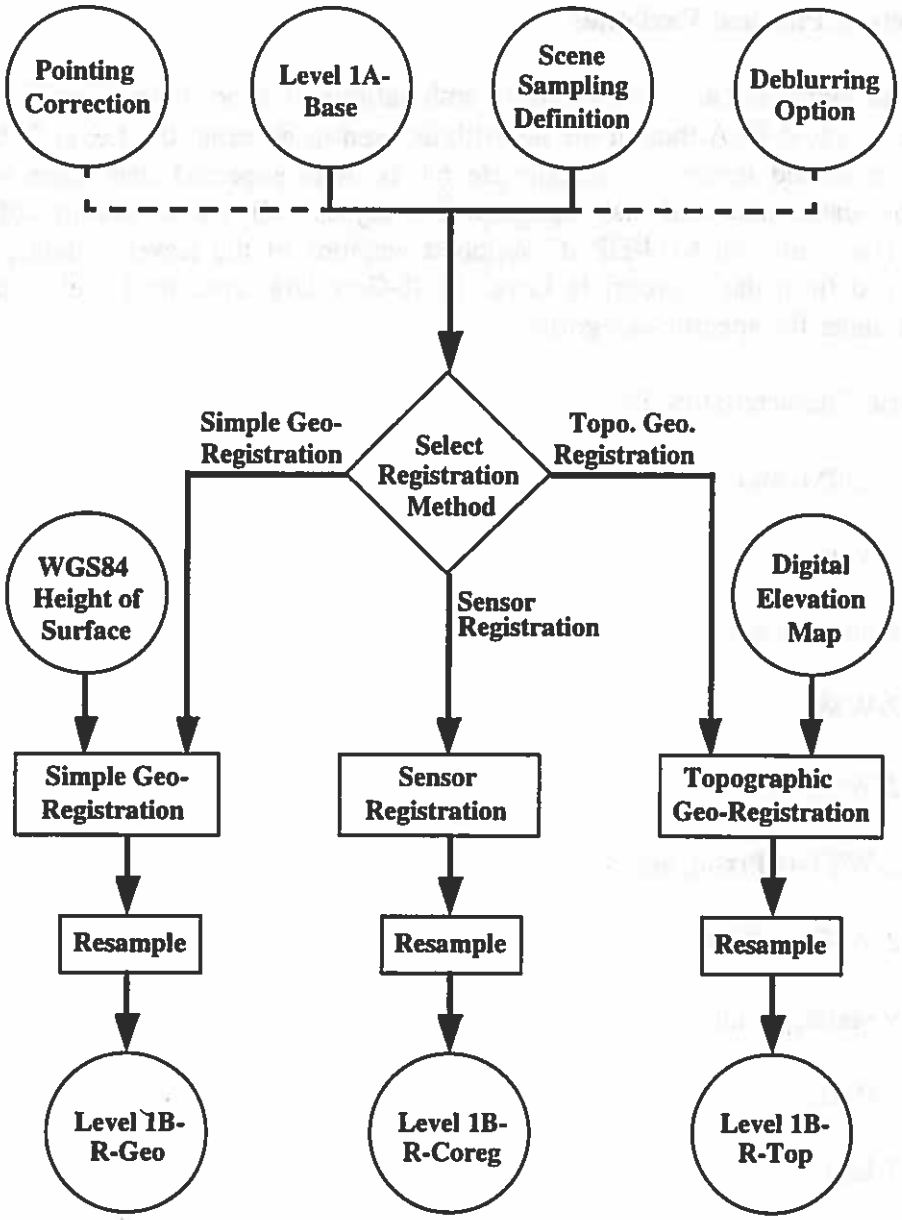

Figure 1-6. Data flow for generating registered data cubes.

Procedures will be provided to allow users to perform their own registrations of Level 1A-Base data products to a surface defined relative to WGS84 or to topographic geo-registration at a minimal cost in resolution. These procedures will contain options for image enhancement to reduce blurring from the optics and motion. The data flow for the Level 1B-R-β data cubes (where β is Coreg, Geo, or Top) is given in Figure1-6. In the resampling step, we found the best results when using the optimum parametric interpolation scheme of Park and Schowengerdt (1983).

1.6 Level 2: Derived Physical Variables

The level 2 data products are all derived from combinations of band images in the co-registered data cubes of Level 1B-R-β. Although the algorithms used to generate the Level 2 data products only assume co-registered images in appropriate bands, it is expected that users will be most interested in geo-located data and that topographic analyses will not be a standard part of the image analysis. Therefore, the MTI-DPAC supplied versions of the Level 2 data products will normally be derived from the appropriate Level 1B-R-Geo data. Specific Level 2 data products will be discussed under the specific categories:

- Atmospheric Characteristics, i.e.,
  - Level 2-CldM, and
  - Level 2-Vap;
- Water Characteristics, i.e.,
  - Level 2-WM,
  - Level 2-WST-α,
  - Level 2-WST-α-Pixon, and
  - Level 2-WST-α-MEM;
- Land and Vegetation, i.e.,
  - Level 2-Refl,
  - Level 2-LST,
  - Level 2-NDVI, and
  - Level 2-Mat.

The relationship of the various Level 1 and 2 data products is illustrated by Figure 1-7.

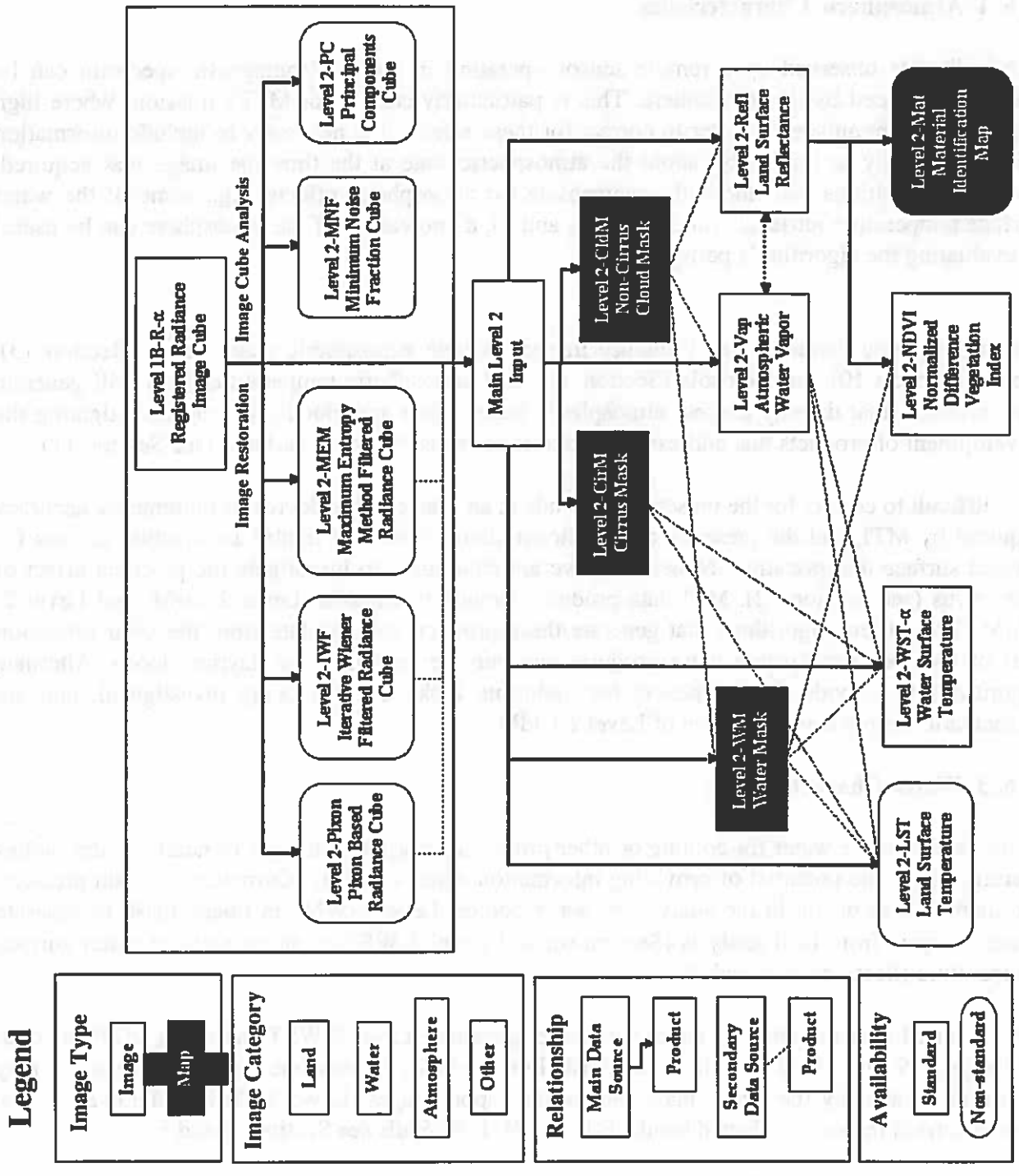

Figure 1-7. Level 2 product relationships.

1. 6. 1 Atmospheric Characteristics

The radiances observed by a remote sensor operating in the electromagnetic spectrum can be greatly influenced by the atmosphere. This is particularly critical for MTI's mission, where high accuracy is prerequisite. In order to correct for these effects it is necessary to include information (either explicitly or implicitly) about the atmospheric state at the time the image was acquired. Even for algorithms that implicitly compensate for atmospheric effects, e.g., some of the water surface temperature retrievals (Sections 4, 5, and 7), a knowledge of the atmosphere can be useful in evaluating the algorithm's performance.

The atmospheric variables that influence images include atmospheric water vapor (Section 13), clouds (Section 10), and aerosols (Section 11), and atmospheric temperature. MTI will generate data products that directly address atmospheric water vapor and clouds. We are investigating the development of products that address atmospheric aerosols over dark surfaces (see Section 11).

It is difficult to correct for the presence of clouds in an image to the degree of radiometric accuracy required by MTI, and the presence of significant cloud cover will render a collection useless for ground surface interpretation. Nonetheless we are continuing to investigate the practical effect of thin cirrus (see Section 12). MTI data products include two masks: Level 2-CirM, and Level 2-CldM. The current algorithms that generate these products rely on data from the solar reflection part of the spectrum so that these products can only be generated for daytime looks. Alternate algorithms to provide these products for nighttime looks are still being investigated, and are expected to supply a night version of Level 2-CldM.

1. 6. 3 Water Characteristics

Many facilities use water for cooling or other processing purposes. Images of nearby water bodies therefore have the potential of providing information about a facility. Currently two data products are identified as useful in the analysis of water bodies: Level 2-WM, an image mask to separate water analysis from land analysis (Section 6); and Level 2-WST-α, an estimate of water surface temperature (Sections 4, 5, and 7).

The standard determination of water surface temperature, Level 2-WST, relies on MTI's thermal IR bands, J-N, combined with the water mask, Level 2-WM. For daytime viewing these bands may be supplemented by the cirrus mask and water vapor images, Level 2-CirM and Level 2-Vap, obtained from the solar reflected bands, E-G and H. For details see Sections 4 and 5.

1. 6. 3 Land and Vegetation

Observation of land surfaces and their vegetation has the potential of providing information on facility activities. Five level 2 data products are currently planned in this category:

- the atmospherically corrected surface reflectance, Level 2-Refl;

- the land surface temperature map, Level 2-LST;
- the normalized difference vegetation index, Level 2-NDVI; and
- the material identification map, Level 2-Mat.

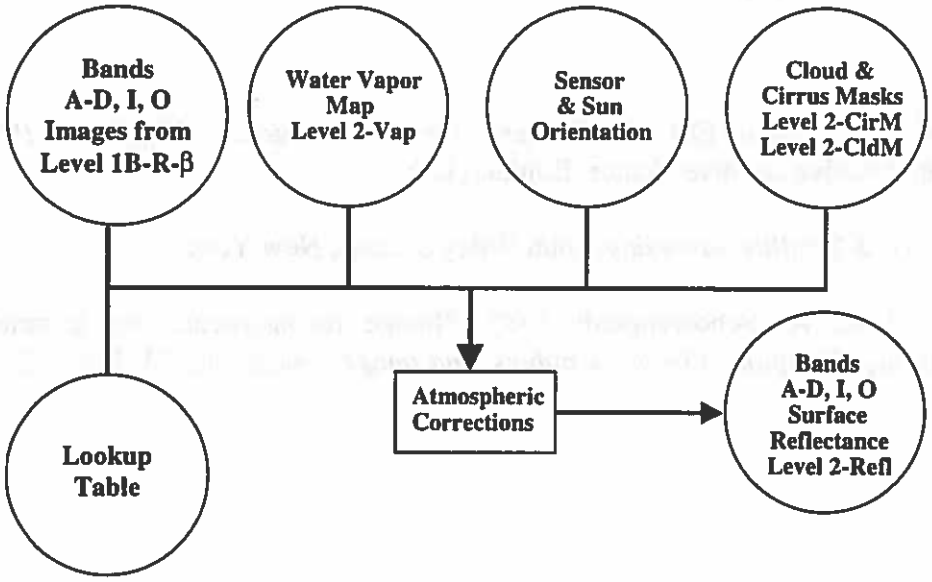

Figure 1-7. Atmospherically corrected reflectances

The atmospherically corrected surface reflectance data set, Level 2-Refl, will be the result of applying simple atmospheric corrections to band radiances in highly transmitting solar reflecting bands. The input will be the Level 1B-R-β data for bands A-D, I, and O and the output will the equivalent reflectances for those bands. The data flow for this product is indicated by Figure1-7.

The land surface temperature data set, Level 2-LST, is discussed in Section 4.

The normalized difference vegetation index, Level 2-NDVI, provides an indicator of vegetation health (Section 14).

The material identification map, Level 2-Mat, will be a special product performed on request only. It will require a list of materials and their spectra (Section 16).

1. 6. 4 General Data Cube Analyses

MTI-DPAC will also provide, on request, three data products related to general data cube analysis, all produced excluding the data in Band H (The cirrus channel); principal components, Level 2-PC; minimum noise fraction analysis, Level 2-MNF; and Inverse Wiener filter analysis, Level 2-IWF, which is normally produced as part of the pixon-based thermal analysis.

1.7 Level 4: Modeling and Detailed Analyses

At this level we plan to offer results of modeling and detailed analyses. Level 4 data model products include: Level 4-ALGE comparison data for water cooling system, (Section 9), and Level 4-RAMS (Section 10). Level 4 data analyses include Level 4-Subpix (Section 8) and Level 4-Veg vegetation health status map (Section 15).

References

Barry, R.G. and A.L. Varani, Eds., 1995: *Earth Observing Science: Highlights 1994*, NSIDC Distributed Active Archive Center, Boulder, CO.

Leick, A., 1990, *GPS Satellite Surveying*, John Wiley & Sons, New York.

Park, S. K., and R. A. Schowengerdt 1983, "Image reconstruction by parametric cubic convolution," *Computer Vision, Graphics, and Image Processing*, **23**, 258-272.

2. CALIBRATION CORRECTION

William B. Clodius and Barham W. Smith

2.1 Introduction and Goal

Many of the processing algorithms for MTI products, e.g., water surface temperature, require high quality relative or absolute calibrations. Therefore radiometric calibration is a major focus of the project. This priority is reflected in the variety of calibration methods that have been implemented in the payload design. Radiometric calibration will be performed for every image and will be the focus of the Level 1A production processing efforts. Other calibration activities, such as determining the post-launch positions of the detectors relative to the optical axis, will occasionally be performed.

The major goals of radiometric calibration correction are

1) to compute the coefficients by which digital numbers from measurement channels are converted to scientific units, and

2) to merge calibration information from several sources into one set of coefficients.

In this section we lay the groundwork for the correction of measured quantities for instrumental response. The scientific basis of the calibration will be discussed in subsection 2.2. This will include an overview of the MTI instrument design, the radiometric model, the ground calibration facilities, and MTI's on-orbit calibration capabilities. Subsection 2.3 will discuss the detailed calibration algorithms: first for the solar reflected bands, then for the thermal infrared bands. These algorithms depend on quantities that can be determined through independent measurements. The procedures used to merge the independent data will be discussed in subsection 2.4. Validation methods will be discussed in the final subsection.

2.2 Scientific Basis

Calibration in the visible (VIS), near infrared (NIR), and short wave infrared (SWIR) is fundamentally different from calibration in the mid-wave and long-wave infrared (MWIR and LWIR) which make up the thermal infrared (TIR). At the shorter wavelengths, radiances are almost invariably due to reflected solar illumination, and radiances should be ratioed to the solar irradiance to infer surface reflectances. Thus calibration in these bands should be relative, and we ratio to the visible reflectance panel (VRP) on the inside of the telescope door. In the TIR, on the other hand, radiance calibration should be absolute, because we are trying to measure the absolute temperature of the heat-emitting ground surface.

The primary factors in calibration of electro-optical systems are:

1) the reflection, transmission, and emission efficiencies of optical elements including mirrors, the window, and filters;

2) the responsivity function for each focal plane array(FPA) pixel, represented in a linear model by a slope and offset;

3) systematic effects in the preamplifiers or other electronic stages;

4) aging of satellite payload components between preflight laboratory calibration and flight observations.

Radiometric calibration will be performed detector element by detector element. The algorithms discussed below will assume a linear response model, so that the calibration for each element can be specified in terms of a simple offset plus linear response. Although the system operation will attempt to ensure that the detectors operate in the linear regime, there is some concern that linear operation cannot be ensured for the LWIR bands, *i.e.*, L, M, and N.

Calibration proceeds through three major stages: 1) characterization of the on-orbit calibration system using both ground based calibration and on-orbit vicarious calibration; 2) characterization of instrument response using the on-orbit calibration system; and 3) conversion of the digitally recorded image response to calibrated responses. Characterization of the on-board calibration system (Figure 2-2) will initially be performed by ground measurements, but will subsequently be maintained by on-orbit cross calibration with ground measurements, with other sensor data, and with deep space looks. Characterization of the instrument response, illustrated by Figure 2-3, depends not only on the on-board calibration system characteristics, its settings, and the resulting detector element response, but also on ancillary data such as the temperature of various system components. Generation of calibrated image data is accomplished in turn by correction of raw digital numbers to this characterized response.

2. 2. 1 Instrument characteristics

Calibration of the MTI imaging system depends on detailed characteristics of the instrument. This system's imaging and radiometric performance is determined by two components that are effectively independent: an optical system that images radiances onto the focal plane; and the focal plane and readout system that converts radiances to digital numbers for on-board storage. The MTI calibration system is designed to provide independent radiometric characterizations of these two components through separate subsystems, an internal on-board calibration system (OBCS) and a system just outside the telescope aperture.

Focal plane response is characterized by an internal set of calibration sources that can be inserted in the optical path after the primary optical elements. This set consists of two lamps for the solar reflective bands, two blackbody sources for the TIR bands, and a narcissus mirror that provides handy near zero radiance points for all bands. The presence of three calibration sources for all bands is sufficient to check the linear behavior of the focal plane. During ground calibration of the payload in our laboratory, we can look for and try to characterize nonlinear behavior.

The optical train is characterized by recording the system's response to sources whose radiances at the aperture are known. The system itself provides two such sources located in the near field: a visible reflectance panel (VRP) for monitoring the solar reflectance bands, and an aperture door assembly (ADA) for monitoring the TIR bands. In addition a variety of deep space and terrestrial targets will be used to characterize the system. The most important of these will be a source-free region of the dark sky, which provides a true zero radiance at the aperture that can be used to assess the system background radiance due to mirrors, the dewar window, and stray light.. Deep space and terrestrial targets will be discussed below in the subsection on validation.

The various operating modes of the MTI calibration system are illustrated by Figure 2-1.

2. 2. 2 Radiometric calibration model

The MTI radiometric model assumes that the radiation incident on the aperture during calibration is uniform within the field of view of the system. Veiling glare and MTF issues can therefore be neglected in the interpretation of calibration sequences. Discussion will also be simplified by neglecting the detailed spectral characteristics of the system, and assuming that averaging reduces shot and quantization noise to negligible levels.

Under the above assumptions, the incidance at the focal plane induced by an external source i at the telescope aperture, in band B on detector pixel D, is given by

$$I^i_{fp,B,D} = \Omega \tau_{op,B} L^i_{ap,B} + I_{bg,B,D}, \tag{2.1}$$

where $L^i_{ap,B}$ is the radiance at the aperture, Ω is a scale factor that depends solely on the optical geometry, $\tau_{op,B}$ is the transmission of the optical system in band B, and $I_{bg,B,D}$ is the incidance due to background thermal emission and scattering by the optical system. For OBCS source j, the warm portions of the optical train are not seen by the focal plane and the incidance is simply that, I^j_{fp}, produced by the source, plus any due to the dewar cold shield (expected to be negligible).

The response of a linear detector pixel D in band B to a focal plane incidance I, where I is either I^i or I^j, is

$$DN_{B,D} = s_{B,D} I_{fp,B,D} + DN_{0,B,D,inc}, \tag{2.2}$$

where DN is the digital number, s is the detector's responsivity per incidance and $DN_{0,inc}$ is the digital offset for incidance. The system response to *radiance at the aperture* is then

$$DN_{B,D} = \sigma_{B,D} L_{ap,B,D} + DN_{0,B,D}, \tag{2.3}$$

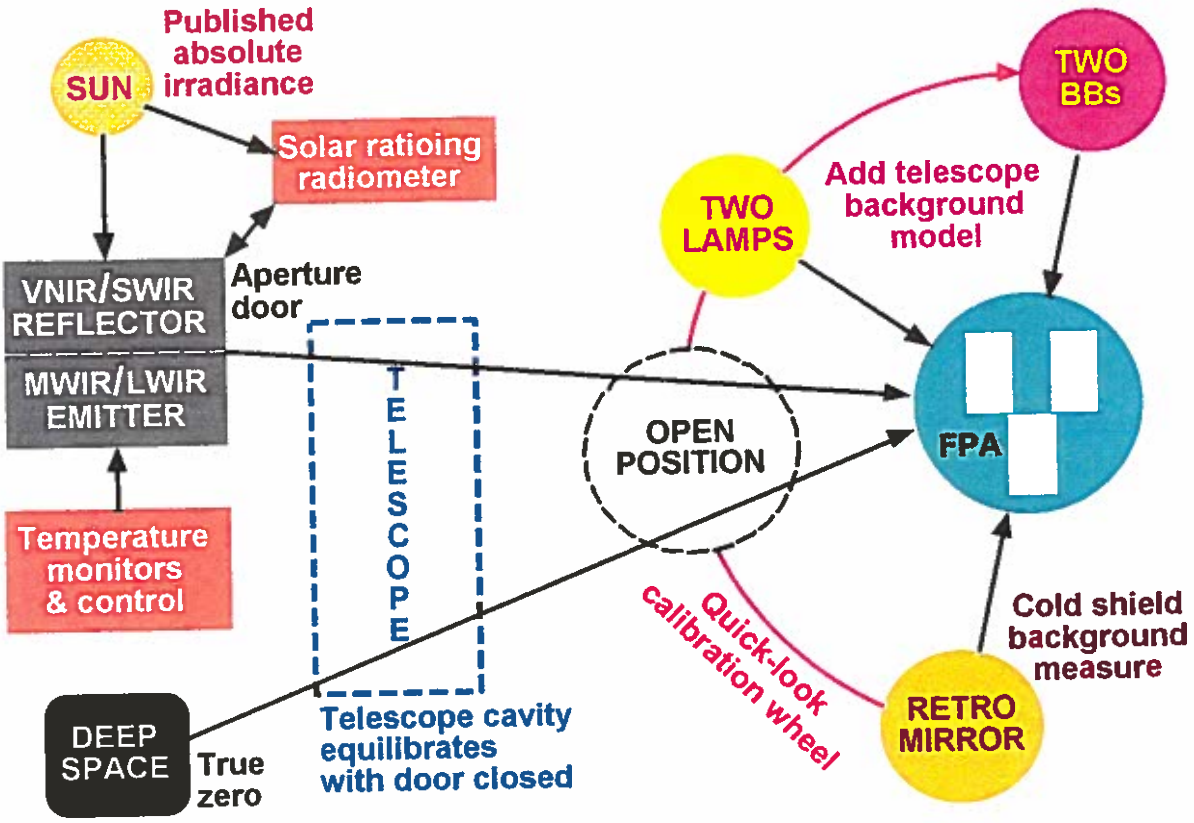

Figure 2-1. Modes of operation of the MTI calibration system. The focal plane array (FPA) is shown on the far right. At right, between the FPA and the telescope cavity, is the OBCS calibration wheel indicated by the semicircular line connecting the two blackbodies ("BBs"), two lamps, and the narcissus mirror. The wheel can rotate to an open position to view the telescope cavity, to expose the FPA to scene radiance from the aperture, stray light scattered from the optical assembly, and thermal radiance from the telescope cavity. Calibration system components beyond the aperture are at left. They include both surfaces of the telescope aperture door, the VRP ("VNIR/SWIR reflector"), whose scattered sunlight is monitored by the solar ratioing radiometer, and the ADA ("MWIR/LWIR emitter"), whose temperature is controlled and monitored, and a deep space look. Except when the ADA is in operation, the telescope cavity cannot be assumed to be in thermal equilibrium, so the temperatures of its various surfaces are monitored and controlled to ensure that temperature drifts are not a significant source of calibration errors in the TIR. Temperatures of the blackbodies and the narcissus mirror are also monitored.

where the responsivity per radiance is

$$\sigma_{B,D} = \Omega \tau_{op,B} s_{B,D}, \tag{2.3}$$

and the offset in digital number is

$$DN_{0,B,D} = s_{B,D} I_{bg,B,D} + DN_{0,B,D,inc}. \tag{2.4}$$

Calibration requires the determination of the system coefficients σ and DN_0. These coefficients are time dependent and ideally should be determined as close as possible in time to any image acquisition. It is impractical, however, to perform the full calibration simultaneous with the measurements, so that some form of interpolation or extrapolation is necessary in the calibration. This is particularly true for the full calibration of the solar reflecting bands which involves maneuvers both to orient the VRP with respect to the sun and to obtain a deep space look. These maneuvers will be performed infrequently because of their large energy costs. Images in the solar reflecting bands will therefore rely on indirect calibration via the OBCS lamps.

2. 2. 3 Preflight laboratory calibration

The MTI payload will be extensively calibrated at Los Alamos in the summer and fall of 1998. Well-known source radiances [traceable to standards at the National Institute of Standards and Technology (NIST)] will be presented to the instrument aperture and digital numbers will be read out and recorded. In addition, the output of the sources that make up the OBCS, the ADA, and the reflectance of the VRP, which are part of the flight instrument package, will be calibrated using the instrument focal plane array (FPA) itself as a transfer radiometer. In this way the on-orbit calibration system is characterized at that point in time. During the months of the laboratory calibration campaign, any secular changes in the OBCS performance can be characterized. In the absence of observed changes, degradation in the OBCS performance must be estimated from known aging effects in the components, e.g. lamps.

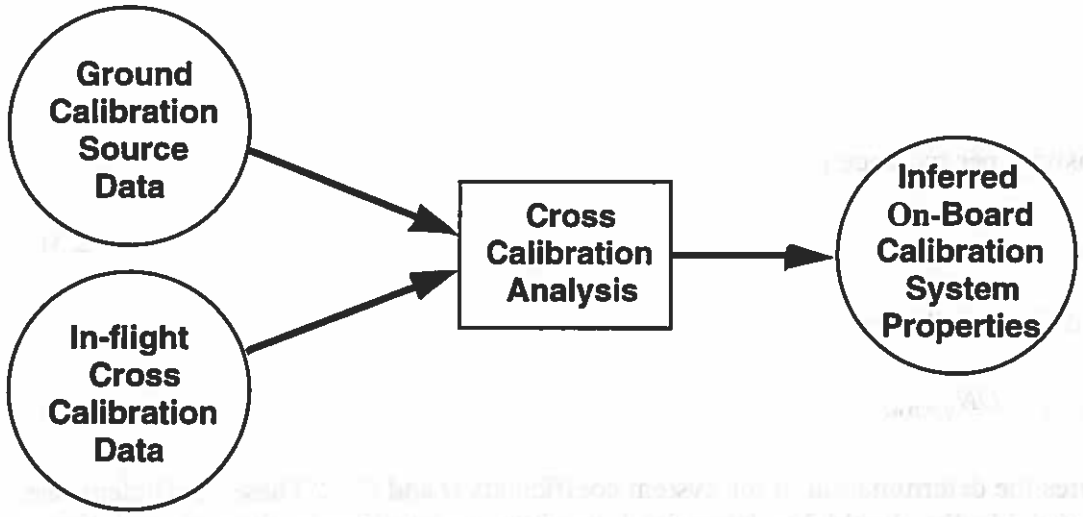

Figure 2-2. Characterization of the on-board calibration system. Preflight calibration in a terrestrial laboratory must be constantly compared to on-orbit calibrations to derive the best coefficients.

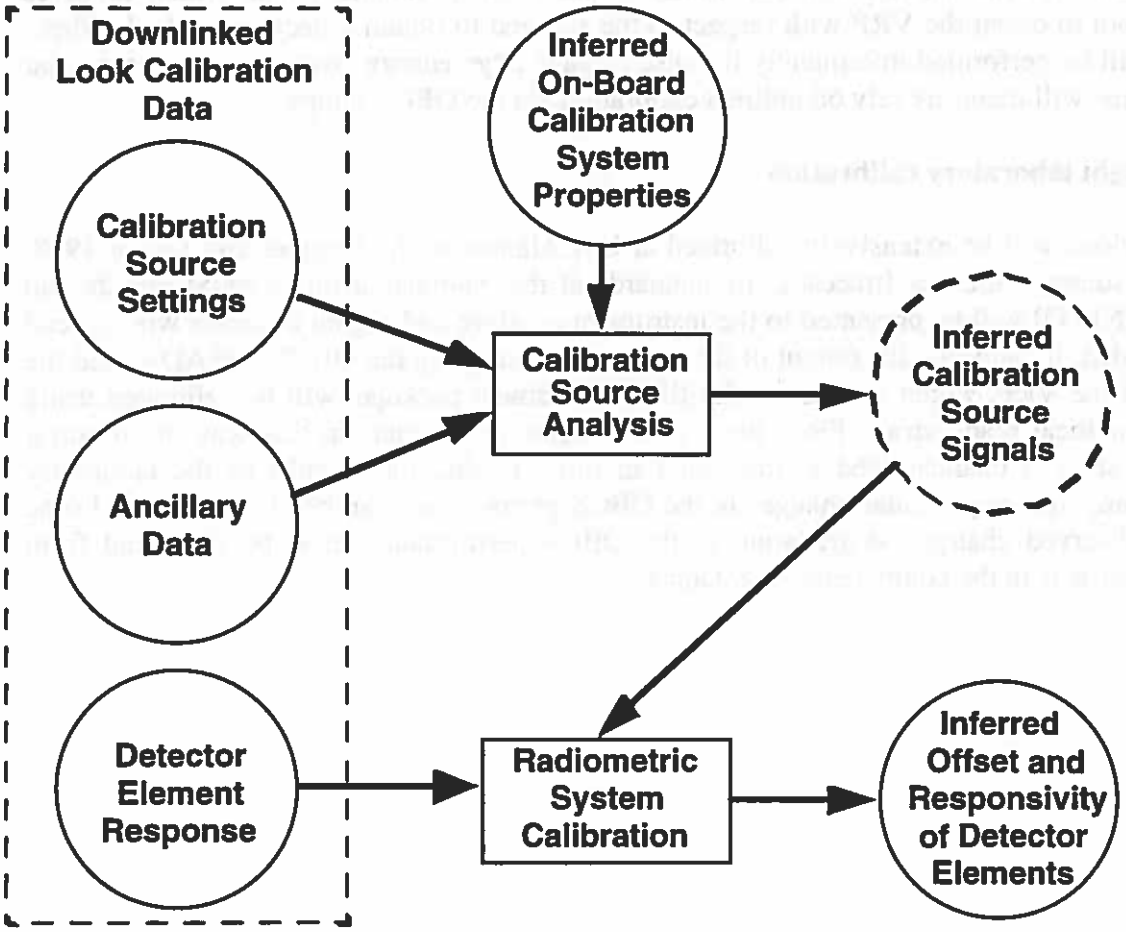

Figure 2-3. Calibration of system response.

2. 2. 4 Calibration on-orbit

Maintenance of the MTI laboratory calibration through transfer to orbit and subsequent on-orbit aging relies on frequent checks. In order to minimize the errors involved in the non-simultaneity of calibration with image acquisition, known sources of drifts have been identified and will be characterized by laboratory measurements or theory. Such sources include detector dependencies on focal plane temperatures, known aging rates for some system components, and the temperature dependence of gray body emissions. These sources will be related to the output of some of MTI's non-imaging sensors, for example various thermistors, and appropriate corrections will be applied to the data before other analyses, so that residual errors are minimized. NASA's Moderate Resolution Imaging Spectroradiometer instrument program (MODIS) has undertaken a rigorous analysis of this problem (Barbieri *et al.* 1998), and we will determine how closely we need to emulate their procedures after we have lived with the MTI payload for some time in our calibration laboratory.

The calibration of the OBCS sources is maintained by vicarious calibration with deep space or terrestrial targets of known radiance. By recording the system's responses to these known sources and performing a linear fit of the response to the inferred radiances, the system coefficients σ and DN_0 can readily be estimated.

The radiant intensity provided by the two OBCS lamps will be related to external radiances by operating the internal OBCS in close temporal proximity with the VRP and a deep space look. These lamps plus the narcissus mirror will comprise a calibration check, and corrections for drifts in the coefficients σ and DN_0 will be estimated by linear fits to the three radiances, and analyses of ancillary data. The incidance provided by the OBCS blackbodies are related to external radiances through NIST-traceable laboratory calibrations and are expected to be stable enough to maintain adequate calibration during the mission's lifetime. The blackbodies and the ADA will operate in close temporal proximity with a scene look, and corrections to short term drifts in the coefficients σ and DN_0 for the TIR bands will be estimated by fits to four radiances, including the most recent deep space look.

2.3 Detailed Algorithms

2. 3. 1 Overview of the algorithms

Data available from MTI represent the response of the system at selected times. This response can be modeled as a function of various system state variables such as the optical system transmission τ_{op}, the VRP albedo, etc. These state variables evolve with time, modifying the response of MTI system components to known sources. The calibration process must merge the responses to a variety of known inputs at known times to infer the values of these state variables at other times (Slater and Biggar 1996).

The current plan is to merge these sources using a Kalman filter (du Plessis 1967; Gelb 1974). Freedman and Byme (1995) have shown that such an approach has great potential for the calibration of satellite-based imaging systems.

A Kalman filter weaves together two separate representations of the system: 1) a model-of the effects of the state variables on observables, and 2) a model of how the state-variables evolve with time. We plan to use a static linear Kalman filter which represents the state vector $\mathbf{x}$ at time t_{k+1} and the system measurement vector $\mathbf{z}$ at time t_k as linear functions of the state vector at time t_k:

$$\mathbf{x}_{k+1} = \phi\mathbf{x}_k + \mathbf{w}_k,$$
$$\mathbf{z}_k = \mathbf{H}\mathbf{x}_k + \mathbf{v}_k, \tag{2.5}$$

where ϕ is the state transition matrix, $\mathbf{w}$ is the dynamics noise vector, $\mathbf{H}$ relates states to measurements and depends on the known input values, and $\mathbf{v}_k$ is the measurement noise vector.

Work is currently proceeding on developing a time-dependent physical model of the state vector. Many details of this model will rely on trends noted during laboratory ground calibration and can only be specified at the end of that process. The majority of state variables represent values that are expected to decrease uniformly with time. Such a state variable, x_j, at time t_{k+1}, will typically be modeled by

$$x_{j,k+1} = \exp\left(-b_j\left(t_{k+1} - t_k\right)\right)x_{j,k} + \varepsilon_{j,k}, \tag{2.6}$$

where $\varepsilon_{j,k}$ is a random variable with zero mean and a variable dependent standard deviation. The work of Freedman and Byme suggests that there is great latitude in specifying a state evolution model.

The remainder of section 2.3 discusses the dependence of the most important observables on the state variables.

2. 3. 2 Conversion to standard response

The detector response is recorded as a digital number, *DN*. The interpretation of this number depends on the settings of the appropriate analog to digital (A/D) converter. Therefore, initial processing converts *DN* back to its equivalent A/D input voltage, *V*. This conversion need not be linear to account for non-linearities either in the A/D conversion or in the focal plane response. This voltage has an offset which, in part, depends on the focal plane temperature, T_{fp}, which is monitored by MTI. Detector performance will be specified relative to a yet to be determined focal plane temperature, $T_{0,fp}$. Laboratory calibrations will determine the focal plane temperature dependence of the offset

$$\delta_{T,fp,B,D} = \left\langle \left(\left\langle V_{0,B,D} \right\rangle_{\Delta T_{fp}} - \left\langle V_{0,B,D} \right\rangle_{T_{0,fp}} \right) \middle/ \Delta T_{fp} \right\rangle, \tag{2.7}$$

where $\Delta T_{fp} = T_{fp} - T_{0,fp}$, $\left\langle V_{0,B,D} \right\rangle_{T_{fp}}$ is the average input voltage offset at T_{fp}, $\left\langle V_{0,B,D} \right\rangle_{T_{0,FP}}$ is the average input voltage offset at $T_{0,fp}$, and the dependence is determined by taking an average over

the various focal plane measurements. The effective input voltage corrected for the focal plane temperature dependence is then

$$V^*_{B,D} = V_{T_0,B,D} = V_{B,D} - \delta_{T,fp,B,D}\Delta T_{fp}. \tag{2.8}$$

Subsequent processing in all bands will be in terms of $V^*_{B,D}$. From this point onwards, the algorithms for the solar reflected bands are different from those for the TIR bands.

2. 3. 3 Reflected solar bands

2. 3. 3. 1 The basic measurement equations

For radiances in the reflected solar bands, the basic measurement equation is

$$V^*_{es,B,D} = L_{es,B,D}\sigma^*_{B,D} + V^*_{0,B,D} \tag{2.9}$$

where

B = Band

D = Detector pixel in band B

es = External source for which data is acquired

$L_{es,B,D}$ = Source spectral radiance

$V^*_{es,B,D}$ = Effective A/D input voltage

$V^*_{0,B,D}$ = Effective A/D input voltage offset

$\sigma^*_{B,D}$ = Radiance responsivy in voltage units

The derivation of calibrated radiances is therefore factored into the derivation of the effective voltage offset and the radiance responsivity. MTI provides several means of quantifying the effects of these values, each applicable on different time scales: the OBCS on time scales comparable to a look; the VRP on time scales of a few tens of scene looks; and external calibration on time scales of a few tens of VRP calibrations. They will be discussed below in the same order

2. 3. 3. 2 Calibration via the OBCS lamps and zero point

The OBCS provides three calibration sources for the solar reflected bands: two lamps and a null radiance, the narcissus mirror. The null radiance is expected to remain true throughout the lifetime of the system. The two lamps and the narcissus mirror will be operated immediately before and after a scene look.

The radiant intensity induced by each lamp, i, can be equivalenced to an effective external radiance value, $L^*_{i,lamp}$. These effective radiance values are referenced to the ground laboratory determined values, $L^*_{i,lamp,lab}$, via the state variables, $\delta_{i,lamp}$.

$$L^*_{i,lamp,cal} = \delta_{i,lamp} L^*_{i,lamp,lab}. \tag{2.10}$$

The lamp radiances as functions of time will be estimated through $\delta_{i,lamp}$ by merging these and other data values as discussed in section 2.3.1.

The estimated OBCS lamp values serve as direct calibration points for scene looks. Detector responses integrated over a sufficiently long interval will have negligible shot and quantization noise. Linear fits to sets of three calibration points separated by time can be interpolated to the time of the scene look to calibrate the look data.

2. 3. 3. 3 Calibration via the VRP

Because orienting the VRP with respect to the sun has a significant cost in time and system energy, it is expected that the VRP will be used to monitor the system only on intervals longer than a few days. In operation the VRP produces an input radiance in band B of

$$L_{R,sun} = E_{sun} \Delta_B BRDF_{0,B} \cos(\theta_{VRP,S}), \tag{2.11}$$

where E_{sun} is the solar band averaged spectral radiance adjusted for the Earth-Sun distance, Δ_B is the relative change in VRP albedo since launch, $BRDF_{0,B}$ is the VRP prelaunch BRDF, and $\theta_{VRP,S}$ is the normal angle of incidance between the sun and the VRP surface.

The VRP monitor (VRPM) provides the direct measure of Δ_B, in the MTI bands A-D. It serves as a solar ratioing radiometer in each reflective band B to both the sun, $R_{B,VRPM,sun}$, and the sunlight reflected by the VRP, $R_{B,VRPM,VRP}$. Then

$$\Delta_B = \frac{R_{B,VRPM,VRP} R_{B,0,VRPM,sun}}{R_{B,VRPM,sun} R_{B,0,VRPM,VRP} \delta_{VRPM}}, \tag{2.12}$$

where $R_{B,0,VRPM,sun} / R_{B,0,VRPM,VRP}$ is the prelaunch value of $R_{B,VRPM,sun} / R_{B,VRPM,VRP}$ and δ_{VRPM} is the change from the prelaunch. The value of δ_{VRPM} is indirectly monitored through external on-orbit calibrations.

VRP calibrations will be immediately preceded and followed by OBCS calibrations. This will provide a close coupling between the state variables δ_{VRPM}, $L^*_{1,lamp,cal}$, and $L^*_{2,lamp,cal}$.

2. 3. 3. 4 On-orbit vicarious calibration

Vicarious calibrations will be performed more rarely than VRP calibrations, since they must be supported by extensive ground truth operations. They will be described by the basic measurement equation

$$V^*_{vc,B,D} = L_{vc,B,D}\sigma^*_{B,D} + V^*_{0,B,D}, \tag{2.13}$$

where

$L_{vc,B,D}$ = Calibration source spectral radiance

$V^*_{EC,B,D}$ = Effective A/D input voltage.

Vicarious calibrations will be immediately preceded and followed by OBCS calibrations. This will provide a close coupling between the state variables $\sigma^*_{B,D}$, $V^*_{0,B,D}$, $L^*_{1,lamp,cal}$, and $L^*_{2,lamp,cal}$.

2. 3. 4 Thermal infrared bands

2. 3. 4. 1 Basic measurement equations

For radiances in the TIR bands, self radiance produced by the instrument complicates the analysis. The basic measurement equation must include this effect which depends on the mode of operation of the sensor

$$V^*_{es,B,D} = (L_{es,B,D} + L_{bg})\sigma^*_{B,D} + V^*_{0,B,D}, \tag{2.14}$$

where

B = Band

D = Detector pixel in band B

es = External source for which data is acquired

$L_{es,B,D}$ = Source spectral radiance

L_{bg} = Background radiance

$V^*_{es,B,D}$ = Effective A/D input voltage

$V^*_{0,B,D}$ = Effective A/D input voltage offset

The derivation of calibrated radiances is therefore factored into the derivation of the effective voltage offset, the radiance responsivity, and the system background. MTI provides several means of quantifying the effects of these values, each applicable on different time scales: the OBCS on

time scales comparable to a look; the ADA on comparable time scales; deep space looks on time scales of a few tens of scene looks; and vicarious calibration on time scales of a few tens of ADA calibrations. They will be discussed below in the same order. The discussion currently assumes that the temperatures of the optical surfaces can be adequately controlled so that their variation from one data acquisition to another need not be explicitly included in the analysis.

2. 3. 4. 2 Calibration via the OBCS blackbodies and narcissus mirror

The OBCS provides three calibration sources for the TIR bands: two blackbodies and a narcissus mirror. Within each band the radiance from the narcissus mirror is expected to behave like a gray body with a small and time-dependent emissivity. While the OBCS is in operation, background sources beyond the mirror, L_{bg}, are not present.

The radiant intensity induced by each OBCS thermal radiance source, i, can be equivalenced to $L^{*}_{i,bb} - L_{OP,bg}$, where $L^{*}_{i,bb}$ is an effective external radiance value, and $L_{OP,bg}$ is the background radiance that would be present if the optical cavity were accessible with an open external aperture. This effective radiance value is related to the radiance, $L^{BB}(T_i)$ of an ideal blackbody at the same temperature, T_i, as the OBCS source, through a scale factor, $S_{i,B}$, which is in turn referenced to the ground laboratory determined values, $S_{i,bb,lab}$, via the state variables, $\delta_{i,bb}$.

$$L^{*}_{i,bb} - L_{OP,bg} = \delta_{i,bb} S_{i,bb,lab} L^{BB}(T_i) \tag{2.14}$$

The estimated OBCS TIR sources serve as direct calibration sources for scene looks. These sources will be operated immediately before and after a scene look, and detector responses will be collected over a sufficiently long time that the averaged response has negligible shot and quantization noise. A linear fit to each of the two sets of three estimated effective radiance values gives estimates of the system response and offset at those two times. These estimates can be interpolated to the time of the scene look to calibrate the look data.

2. 3. 4. 3 Calibration via the ADA

The focal plane incidance induced by ADA can be equivalenced to an effective external source radiance

$$\left(L_{ES} + L_{bg}\right) = \left(L_{ADA} + L'_{ADA,bg} + L_{OP,bg}\right), \tag{2.15}$$

where L_{ADA} is the radiance directly produced by the door thermal emissions, $L_{OP,bg}$ is the background radiance that would be present if the external aperture were open, and $L'_{ADA,bg}$ is the additional background radiance due to the finite reflectance of the ADA. The ADA thermal emissions are related to the ADA temperature, T_{ADA}, through the relations

$$L_{ADA} = \varepsilon_{ADA} L^{BB}(T_{ADA}), \tag{2.16}$$

where ε_{ADA} is the effective door emissivity. The current mdel assumes that ε_{ADA} can be assumed to be a constant during the system lifetime. The additional ADA background radiance is modeled as

$$L_{ADA,bg} = (1-\varepsilon_{ADA}) S_{ADA}, \tag{2.17}$$

which is related to the laboratory measured value via the state variable, $\delta_{ADA,bg}$,

$$S_{ADA} = \delta_{ADA,bg} S_{ADA,lab}. \tag{2.18}$$

More sophisticated models for both the ADA thermal emissions, and the ADA reflectance contribution to the background are under consideration.

ADA response measurements will always occur in close temporal proximity with OBCS thermal calibrations.

2. 3. 4. 4 Calibration via a deep space look

MTI will be periodically oriented toward a dark region of the sky free of significant cosmic sources and data will be acquired for an effective zero input radiance

$$V^{*}_{0.ex,B,D} = L_{bg} \sigma^{*}_{B,D} + V^{*}_{0,B,D}, \tag{2.19}$$

where the subscript *ex* indicates that the measurement is for zero radiance at the external aperture, not zero incidance on the focal plane. This measurement is primarily intended to track the system background radiance, which depends on the temperature of various surfaces in the telescope cavity. Because surfaces warm enough to contribute significant radiances are at similar temperatures, the current model lumps these surfaces together and models the background radiance by

$$L_{bg} = \varepsilon_{bg,eff} L^{BB}(T_{bg,eff}), \tag{2.20}$$

where $\varepsilon_{bg,eff}$ is an effective emissivity and $T_{bg,eff}$ is an effective temperature that will be determined through an as yet unspecified algorithm. Changes in background radiance will be related to laboratory measurements through the state variable, δ_{bg}, which relates the current value of $\varepsilon_{bg,eff}$ to the laboratory measured value $\varepsilon_{bg,eff} = \delta_g \varepsilon_{bg,eff,lab}$.

Note a dark sky look will be bracketed by OBCS and ADA calibrations to provide close association with other state variables.

2. 3. 3. 4. 5 On-orbit vicarious calibration

Vicarious calibrations will be performed more rarely than dark sky calibrations, because of the necessity for ground truth operations, and will be described by the basic measurement equation

$$V^*_{vc,B,D} = \left(L_{vc,B,D} + L_{op,bg}\right)\sigma^*_{B,D} + V^*_{0,B,D}, \tag{2.21}$$

where

$L_{vc,B,D}$ = Calibration source spectral radiance

$L_{op,bg}$ = Open aperture background spectral radiance

$V^*_{0,B,D}$ = Effective A/D input voltage offset

Vicarious calibrations will be immediately preceded and followed by OBCS and ADA calibrations.

2.4 Error Budget

The temperature accuracy requirements for MTI are derived from studies of applications. The error budget was equally divided between the error due to imperfect exploitation algorithms and the error due to imperfect calibration.

2.5 Validation Plan

The radiometry requirements for MTI are challenging. In order to ensure that these requirements are met it is necessary to have available several different calibration methods to validate MTI's performance. These methods must provide known radiances at the on-orbit aperture of the system, independent of the VRP and ADA.

Such radiances are provided through vicarious calibration, where the top of atmosphere (TOA) radiance produced by a scene is characterized in various MTI bands. This characterization involves some combination of: 1) measurements of ground properties and atmospheric state by a ground truth team, after the manner of Biggar *et al.* (1994) and Slater *et al.* (1996), to estimate radiances at top of atmosphere; 2) measurements from an aircraft (Abel *et al.* 1993); and 3) estimation of top-of-atmosphere radiance by other satellite-based sensors, all concurrent with an MTI image acquisition for the site of interest. In addition the observation of selected deep space fields will be used to supplement this data.

Ground truth measurements can adequately cover only a small portion of the site as imaged by MTI. The utilization of this data therefore requires particularly careful and detailed registration of the pixels in MTI bands with scene points chosen for vicarious calibration. This registration requirement depends on the site's uniformity and sites with extensive uniform surfaces are desirable.

Ground truth measurements must occur in the lower atmosphere. The measurements must be extrapolated to the satellite using an atmospheric radiation transport code. Error analysis must include any errors due to these radiation transport calculations. High altitude sites are less subject to these errors and so are particularly desirable for vicarious calibrations.

Ground truth measurements will often be indirect. The BRDF, and not the radiance, of scene components of interest will be directly measured and the radiances used in the calibrations will be those predicted using a radiation transport code. Error estimates for such data must include not only the errors in the BRDF measurements, but also any errors in the modeling of the radiation transport.

Comparison of MTI data with measurements by aircraft-based sensors benefits from the higher altitude of the aircraft sensor. Errors due to radiation transport calculations are greatly reduced in comparisons with the data from such systems. But the analysis must both adjust for band differences between the aircraft and MTI sensors and identify those portions of the data from the two systems that are most similar in time of acquisition and look angle, and associate appropriate error estimates for any residual differences. Corrections for band differences appear to be most straightforward for aircraft-based hyperspectral sensors, because MTI spectral bands can be synthesized from fine resolution spectral channels.

Differences in look angle and band systems are the most significant complications in the comparison of MTI data with measurements by other satellite based imaging systems. There are currently no hyperspectral sensors in orbit, so that band comparisons with different satellite systems will be approximate. Fixed satellite orbits make it impractical for other such systems to achieve close alignment in both time of acquisition and look angle with data acquisitions by MTI..

The observation of deep space fields is planned as part of the MTI on-orbit calibration. A few stars have been identified as candidates for calibration in the infrared. In addition, the Moon may become a useable calibration source should a current ground-based telescope program (Kieffer and Widley 1992, 1996) achieve its goal of characterizing the moon's brightness to about 2%. Because of libration and its non-uniform and non-lambertian surface, the Moon's radiance is difficult to characterize, and current knowledge is insufficient for MTI's needs.

Each of the validation methods described above has strengths and weaknesses. Collectively, when implemented at appropriate sites, they should provide the data to maintain the calibration of the MTI imaging system. Appropriate sites have been identified and planning is underway for the data collection once the system is in operation. With this data in hand, the aging of system components can be modeled to derive new formulae for computing future sets of calibration coefficients.

2.5 References

P. Abel, B. Guenther, R. Galimore, and J. Cooper, 1993: Calibration results for NOAA-11 AVHRR channel-1 and channel 2 from congruent aircraft observations, *J. Atmos. Oceon. Tech.*, **10**, pp. 493-508.